Geoid variance reduction for optimized models

Results are shown for viscosity models optimized with three free parameters

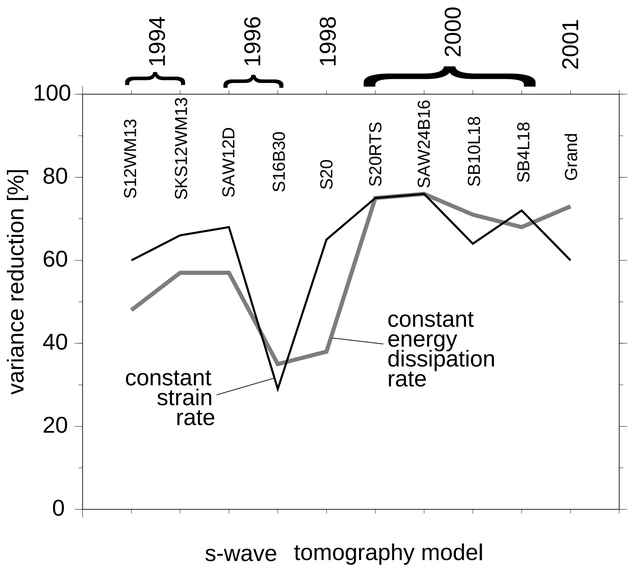

As an example, we compare the

predicted geoid

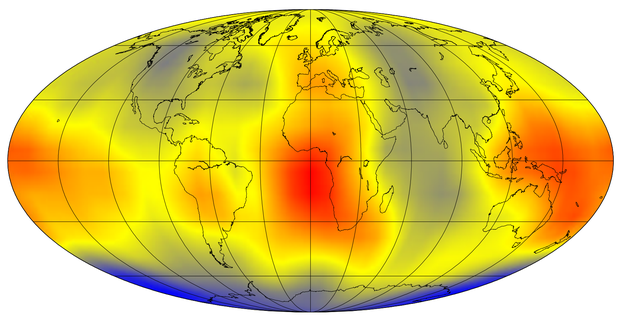

for tomographic model SB4L18 and a viscosity model of the "constant strain rate" type, optimized with three free parameters, with the

observed geoid

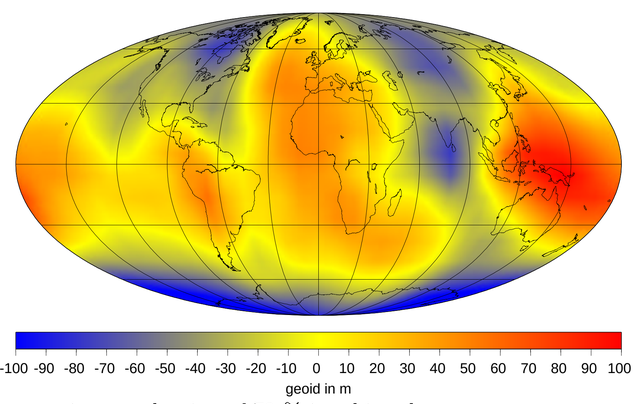

In this example, a variance reduction of 72 % is achieved

Advected heat flux profiles for optimized models

Again, results are shown for viscosity models optimized with three free parameters. Profiles are only plotted for models that achieve a geoid variance reduction of $> 70\%$.

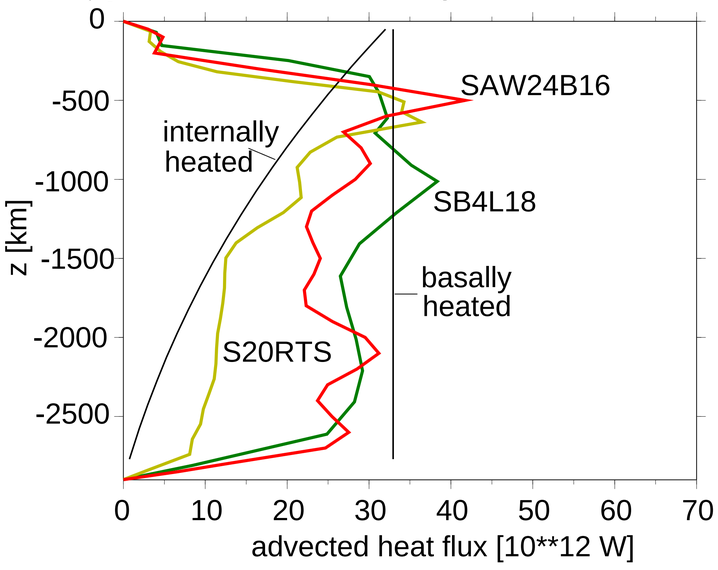

Results for optimized viscosity models of the "constant strain rate" type. Two of the models shown look more like a mantle mainly heated from below, one models looks more like a mantle heated from within.

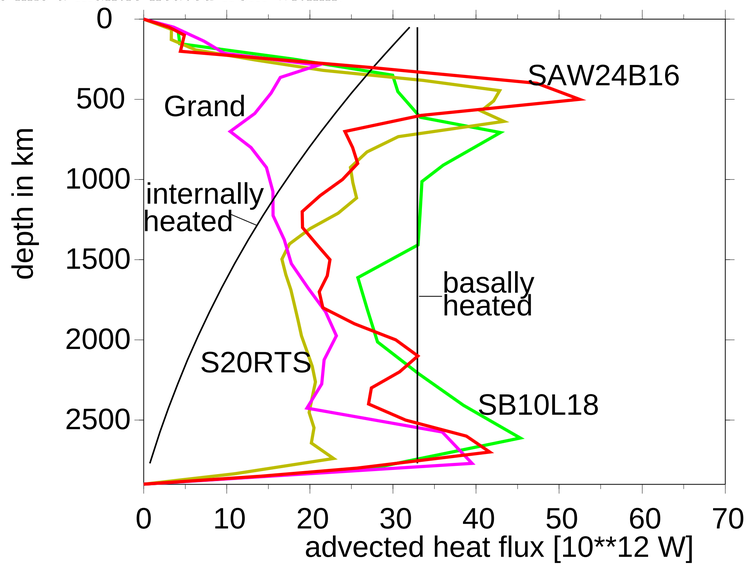

Results for optimized viscosity models of the "constant energy dissipation rate" type. These models tend to overpredict heat flux close to the CMB. We therefore concentrate in the following on the "constant strain rate" type.

Optimized viscosity profiles

Results are shown for profiles of the "constant strain rate" type.

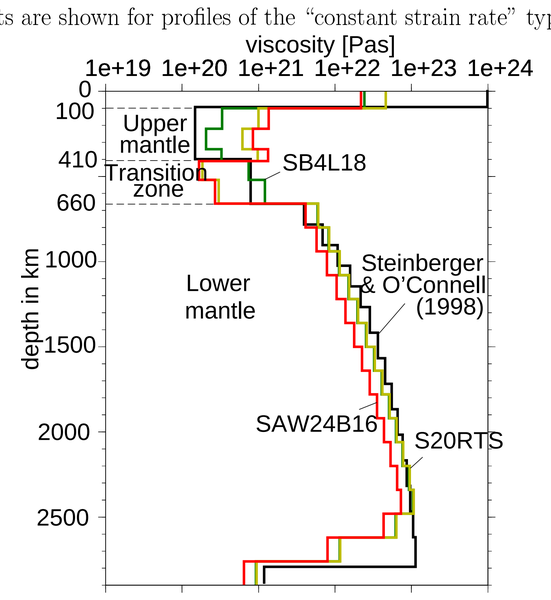

Viscosity profile optimized with three free parameters. Profiles are only plotted for models that achieve a geoid variance reduction of $> 70\%$. The green profile looks very similar to a viscosity model previously proposed based on models of hotspot motion, and features a low-viscosity "asthenosphere". It also gives a good geoid variance reduction of $\sim 70\%$ for the other two models. It is therefore our preferred model.

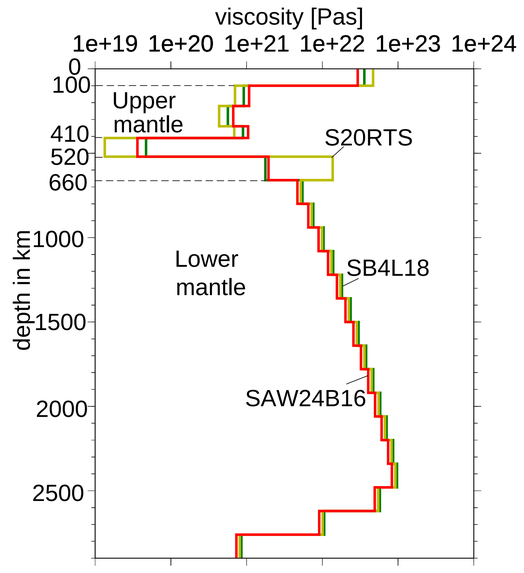

Viscosity profile optimized with four free parameters. Viscosities in the upper and lower transition zone are independently varied. Profiles are only plotted for models that achieve a geoid variance reduction of $> 75\%$. All models favour a low-viscosity "notch". It is however not clear whether the slight increase in variance reduction is sufficient evidence for such a feature.

Predicted lithospheric stresses

As an example, we compare the stresses predicted based on model S20RTS (Ritsema and Van Heijst, 2000), plus lithospheric contributions assuming isostasy, to an interpolation from observed stress directions (Bird and Li, 1996).

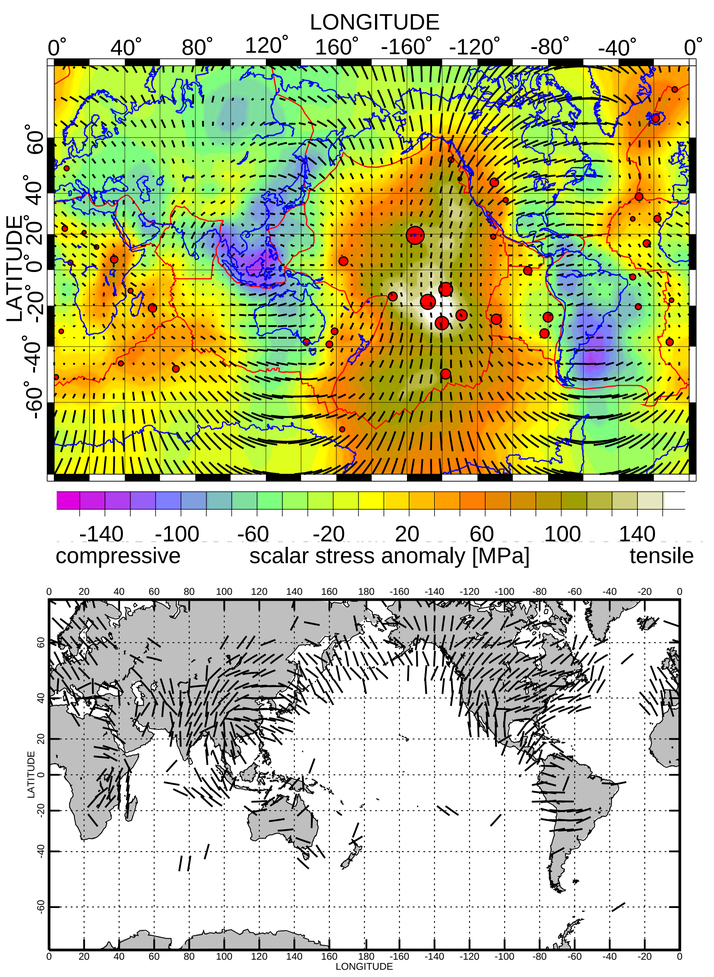

In this example, the mean azimuth error is 26.3 degrees.

Conclusions and Outlook

Conclusions

- A geoid variance reduction > 70 % was achieved for flow fields based on three different recent tomography models
- The same three models give acceptable heat flux profiles. Results indicate that the mantle is heated largely from below, but do not tightly constrain the percentage of internal heating, because different tomography models have different amplitude.
- The angular misfit of predicted and observed lithosphere stresses is 26 to 30°.
- Optimize models feature a viscosity increase by a factor 400 - 600 throughout the mantle.

Outlook

We plan to

- use consistent boundary conditions for geoid and heat flow modelling
- include lateral viscosity variations
- improve the treatment of lithospheric effects (e.g., compositional versus thermal origin of seismic velocity variations)
- extend to time-dependent modelling (allowing us to use hotspot tracks, tpw etc. as modelling constraints)

Acknowledgement

Figures were prepared using GMT graphics (Wessel and Smith, 1995). We thank S. Grand for supplying his tomographic model prior to publication, and P. Bird for a postscript figure.

Literature

P. Bird, Y. Li, Interpolation of principal stress directions by nonparametric statistics: Global maps with confidence limits, J. Geophys. Res. 101 (1996) 5435-5443.

A.R. Calderwood, Mineral Physics Constraints on the Temperature and Composition of the Earth's mantle, Ph.D. thesis, University of British Columbia, Dept. of Earth and Ocean Sciences (1999), 1200 pp..

G. Ekström, A.M. Dziewonski, The unique anisotropy of the Pacific upper mantle, Nature, 394 (1998) 168-172.

S.P. Grand, R.D. Van der Hilst, S. Widiyantoro, Global seismic tomography: A snapshot of convection in the Earth, GSA Today 7 (1997) 1-7.

Ita, J., and Stixrude, L., Petrology, Elasticity, and Composition of the Mantle Transition Zone, J. Geophys. Res., 97 (1992) 6849-6866.

X.D. Li, B. Romanowicz, Global Mantle Shear-Velocity Model Developed Using Nonlinear Asymptotic Coupling Theory, J. Geophys. Res., 101 (1996) 22245-22272.

Liu, X.-F., and A. M. Dziewonski, Lowermost mantle shear wave velocity structure, EOS Trans. AGU, 75, Fall Meet. Suppl. (1994) 663.

G. Masters, G. Laske, H. Bolton, A. Dziewonski, The relative behavior of shear velocity, bulk sound speed, and compressional velocity in the mantle: implications for chemical and thermal structure, in: S. Karato (Ed.), Seismology and Mineral Physics, Geophys. Monogr. Ser., 117, AGU, Washington, D. C., 2000, pp. 63-87.

C. Mégnin, B. Romanowicz, The shear velocity structure of the mantle from the inversion of of body, surface and higher modes waveforms, Geophys. J. Int, 143 (2000) 709-728.

J.X. Mitrovica, A.M. Forte, Radial profile of mantle viscosity: Results from the joint inversion of convection and postglacial rebound observables, J. Geophys. Res. 102 (1997) 2751-2769.

J.X. Mitrovica, Haskell [1935] revisited, J. Geophys. Res. 101 (1996) 555-569.

J. Ritsema, H.J. Van Heijst, Seismic imaging of structural heterogeneity in Earth's mantle: Evidence for large-scale mantle flow, Science Progress, 83 (3) (2000) 243-259.

B. Steinberger, and R.J. O'Connell, Advection of plumes in mantle flow: Implications for hotspot motion, mantle viscosity and plume distribution, Geophys. J. Int. 132 (1998) 412-434.

W.-J. Su, R.L. Woodward, A.M. Dziewonski, Degree 12 model of shear velocity heterogeneity in the mantle, J. Geophys. Res. 99 (1994) 6945-6980.

P. Wessel, W.H.F. Smith, New version of the Generic Mapping Tools released, EOS Trans. AGU 76 (1995) 329.